The Reversible Two-State Unfolding of a Monocot Mannose-Binding Lectin from Garlic Bulbs Reveals the Dominant Role of the Dimeric Interface in Its Stabilization†

Kiran Bachhawat,* Mili Kapoor, Tarun K. Dam, and Avadhesha Surolia*

Molecular Biophysics Unit, Indian Institute of Science, Bangalore-560012, India

Received December 6, 2000; Revised Manuscript Received March 5, 2001

ABSTRACT: *Allium sativum* agglutinin (ASAI) is a heterodimeric mannose-specific bulb lectin possessing two polypeptide chains of molecular mass 11.5 and 12.5 kDa. The thermal unfolding of ASAI, characterized by differential scanning calorimetry and circular dichroism, shows it to be highly reversible and can be defined as a two-state process in which the folded dimer is converted directly to the unfolded monomers ($A_2 \leftrightarrow 2U$). Its conformational stability has been determined as a function of temperature, GdnCl concentration, and pH using a combination of thermal and isothermal GdnCl-induced unfolding monitored by DSC, far-UV CD, and fluorescence, respectively. Analyses of these data yielded the heat capacity change upon unfolding (ΔC_p) and also the temperature dependence of the thermodynamic parameters, namely, ΔG, ΔH, and ΔS. The fit of the stability curve to the modified Gibbs−Helmholtz equation provides an estimate of the thermodynamic parameters ΔH_g, ΔS_g, and ΔC_p as 174.1 kcal mol^{-1}, 0.512 kcal mol^{-1} K^{-1}, and 3.41 kcal mol^{-1} K^{-1}, respectively, at $T_g = 339.4$ K. Also, the free energy of unfolding, ΔG_s, at its temperature of maximum stability ($T_s = 293$ K) is 13.13 kcal mol^{-1}. Unlike most oligomeric proteins studied so far, the lectin shows excellent agreement between the experimentally determined ΔC_p (3.2 ± 0.28 kcal mol^{-1} K^{-1}) and those evaluated from a calculation of its accessible surface area. This in turn suggests that the protein attains a completely unfolded state irrespective of the method of denaturation. The absence of any folding intermediates suggests the quaternary interactions to be the major contributor to the conformational stability of the protein, which correlates well with its X-ray structure. The small ΔC_p for the unfolding of ASAI reflects a relatively small, buried hydrophobic core in the folded dimeric protein.

Determination of the conformational stability of a protein is critical for the appropriate knowledge of the physical interactions that stabilize the protein. The stability estimate of a protein is very often based on the analysis of denaturant-induced or thermally induced unfolding transitions measured either spectroscopically or calorimetrically (*1*−*5*).

The choice of protein is an important factor in determining the physical interactions underlying its conformational stability and folding pathway. The criteria, normally suited for equilibrium denaturation and kinetic studies, are the reversibility and also knowledge of the three-dimensional structure of the protein. Work along these lines has largely focused on small monomeric proteins, which have provided a wealth of information on the stability and folding pathways of proteins (*6*, *7*). A large repertoire of proteins, however, exist as oligomers, and hence it becomes imperative to address questions pertaining to the role of subunit−subunit interactions for the overall stability and integrity of oligomeric proteins (*8*).

The crystal structures of representative monocot mannose-binding lectins, namely, the snowdrop (*Galanthus nivalis*) (*9*), daffodil (*Narcissus pseudonarcissus*) (*10*), bluebell (*Scilla campanulata*) (*11*), amaryllis, (*Hippeastrum hybrid*) (*12*), and garlic (*Allium sativum*) (*13*) lectins, classify them as part of a new mannose-specific lectin superfamily. These bulb lectins are an extended superfamily of structurally and evolutionarily related proteins identified so far in Amaryllidaceae, Alliaceae, Araceae, Orchidaceae, Liliaceae, and the recently reported Iridaceae families (*14*, *15*). Their subunits possess a novel interrelated pseudo-3-fold symmetry having three 4-stranded antiparallel β-sheets oriented as 3 sides of a trigonal prism forming a 12-stranded β-barrel, referred to as the β-prism II fold (Figure 1). These 12 strands are positioned perpendicular to the plane of symmetry unlike other known all-β-folds: β-prism I [e.g., Jacalin (*16*)] and the β-trefoil [e.g., amaranthin (*17*)] fold (*13*). The core of this β-barrel is lined with conserved hydrophobic side chains, which stabilize the fold.

The subject of our study is the mannose-specific protein from the bulbs of garlic, which accumulate two types of

† The VPDSC facility was funded by a grant from the Department of Science and Technology, Government of India, under their IRHPA program, to A.S. K.B. is a Senior Research Fellow supported by the University Grants Commission, and T.K.D. was part of the Postdoctoral Fellow program of the Department of Biotechnology, Government of India under a grant to A.S.

* Correspondence should be addressed to this author at the Molecular Biophysics Unit, Indian Institute of Science, Bangalore-560012, India. Fax: 91-80-3600535/360 0683. Tel: 91-80-3092389. E-mail: surolia@mbu.iisc.ernet.in, kiran@mbu.iisc.ernet.in.

10.1021/bi0027783 CCC: $20.00
Published on Web 05/25/2001

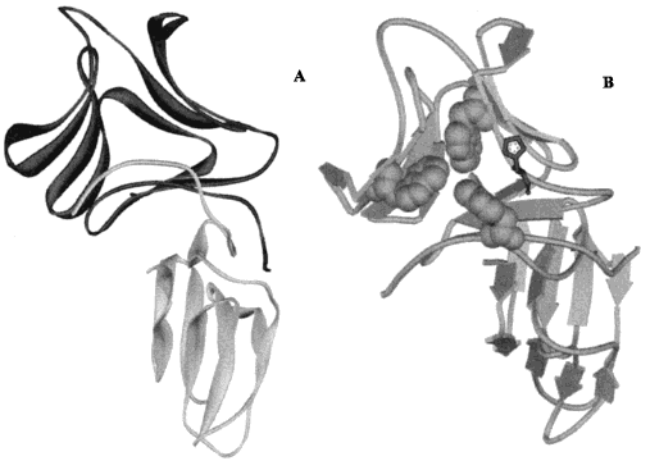

FIGURE 1: (A) Schematic of the three-dimensional structure of the heterodimeric ASAI solved at 2.4 Å (PDB code 1bwu). (B) Orientations of the three tryptophans (Trp41 and Trp74 and Trp103 from the dimer-related subunit) forming the hydrophobic core of the ASAI monomer are highlighted in the β-prism fold II in CPK notation. The His77 is shown in ball-and-stick. Prepared using WebLab ViewerLite 3.5.

mannose-binding lectins: heterodimeric, *Allium sativum* agglutinin I (ASAI),[1] and homodimeric, ASAII (*18*). Interestingly though, snowdrop lectin (GNA) and garlic lectin (ASA) exhibit identical subunit organization and share 70% homology at the amino acid level; GNA exists solely as a tetramer and ASAI only as a dimer. A thermodynamic analysis of the unfolding behavior of these lectins can provide the key to assess the stability and its effect on the oligomerization of these proteins (*19*).

In this paper, we report the structural stability of ASAI using high-precision differential scanning calorimetry (DSC), fluorescence, and circular dichroism spectroscopy (CD) to gain insight into its unfolding behavior. This investigation shows the unfolding of garlic lectin to follow a two-state process, where unfolding and dissociation proceed hand-in-hand. This is well explained in terms of the equilibrium population of folded dimers and unfolded monomers to obtain the estimates of its conformational stability. The high degree of reversibility of the denaturation of this protein, seen both calorimetrically and spectrophotometrically, as well as knowledge of its three-dimensional structure makes this an amenable system for following protein folding pathway(s) in multimeric proteins. In addition, the thermodynamic parameters evaluated conformed to the linear extrapolation model (LEM) for protein−denaturant interactions, which incidentally is the first report wherein LEM has been tested on an oligomeric all-β-sheet protein.

EXPERIMENTAL PROCEDURES

Materials. Mannose was obtained from Sigma. Guanidine hydrochloride (GdnCl) was procured from USB. All other chemicals used were of analytical grade. Stock GdnCl solutions were prepared in 20 mM PBS, pH 7.5, and its molarity was determined by the refractive index measured on the Abbe refractometer as described by Pace et al. (*20*).

[1] Abbreviations: ASAI, *Allium sativum* agglutinin I; GNA, *Galanthus nivalis* agglutinin; DSC, differential scanning calorimetry; CD, circular dichroism; GdnCl, guanidine hydrochloride; PBS, phosphate-buffered saline; ΔH_c, calorimetric enthalpy; ΔH_v, van't Hoff enthalpy.

Protein Purification. ASAI was purified to homogeneity as described previously (*21*).

Differential Scanning Calorimetry Measurements. DSC scans for measuring the change in excess heat capacity as a function of temperature were performed using a Microcal Inc. VP-DSC heat conduction scanning microcalorimeter, which consists of two fixed 0.5073 mL cells, a reference cell and a sample cell. The DSC scans were carried out as a function of protein concentration, scan rate, and pH. The protein concentrations used were 4, 8, 16, 32, and 64 μM. DSC measurements at varying pH from 5.0 to 8.0 were carried out. Citrate phosphate buffer (20 mM) was used for the pH range 5.0−6.5, while for pH ranging from 7.0 to 8.0, the samples were equilibrated in 20 mM PBS. All solutions used for DSC were degassed prior to being loaded onto the calorimeter. Reversibility of the thermal transitions was examined by rescanning the samples. Data were analyzed using the ORIGIN DSC software provided by Microcal Inc. for a two-state $A_2 \leftrightarrow 2U$ process. T_m and T_p are the temperature of half of the transition peak area and the temperature at which the transition peak is at its maximum, respectively. The calorimetric enthalpy (ΔH_c) is determined by the area under the transition, while the van't Hoff enthalpy (ΔH_v) was determined by fitting the data using the Origin software assuming a $A_2 \leftrightarrow 2U$ type transition. The ratio $\Delta H_c/\Delta H_v$ provides the cooperativity of the transition (*22*, *23*).

Fluorescence Measurements. The fluorescence measurements were made on a JASCO FP777 spectrofluorometer in a 1 cm water-jacketed cell. The excitation and emission wavelengths were fixed at 280 and 359 nm with slit widths for both monochromators set at 5 nm. Each measurement was an average of three readings. For protein concentration dependence, 5 and 15 μM samples were equilibrated at the desired temperature for 12 h prior to measurement. Isothermal GdnCl-induced denaturation measurements were made at nine temperatures from 283 to 323 K, using 5 μM protein sample in 20 mM PBS, pH 7.5.

CD Measurements. CD recordings were made on a Jasco J-715 spectropolarimeter interfaced to a microcomputer for automatic data collection and analysis. Temperature scans were performed by scanning continuously from 20 to 90 °C in a 1 mm rectangular quartz cuvette monitored at 216 nm. The data were collected with a bandwidth of 1 nm, response time of 8 s, and scan speed of 10 nm/min. Protein samples were incubated for 8−10 h at the desired denaturant (GdnCl) concentration before measurements were taken to attain equilibrium. Concentrations of protein used were 1, 2, 5, 10, and 15 μM. Each data point was an average of 4 accumulations. Reversibility of protein unfolding was checked by return of the complete spectrum upon thermal unfolding followed by subsequent cooling to ambient temperature.

Data Analysis. Protein stability is defined by Becktel and Schellman (*24*) as a function of the free energy of unfolding (ΔG) with respect to temperature. For dimeric protein, T_m and T_p obtained from DSC depend on the concentration of the protein subunits whereas the concentration-independent Gibbs−Helmholtz equation is obtained by using T_g as a reference temperature, where T_g is the temperature at which $\Delta G_T = 0$. ΔG was calculated from the experimental transition enthalpies at T_m (ΔH_T), T_g, and ΔC_p, which is the difference in heat capacity between the native and unfolded states, using the modified Gibbs−Helmholtz equation (*25*):

$$\Delta H_T = \Delta H_g + \Delta C_p(T - T_g) \quad (1)$$

$$\Delta S_T = \Delta S_g + \Delta C_p \ln(T/T_g) \quad (2)$$

$$\Delta G = \Delta H - T\Delta S \quad (3)$$

$$\Delta G_T = \Delta H_g(1 - T/T_g) - \Delta C_p(T_g - T) - \Delta C_p T \ln(T/T_g) \quad (4)$$

ΔH_g and ΔS_g are the values of ΔH and ΔS at T_g. For solvent denaturation curves, the key parameter is the '*m*' value, defined as the gradient of change in the folding free energy with molar denaturant concentration. According to LEM (*26*, *27*), the changes in ΔG, ΔH, ΔS, and ΔC_p that accompany protein unfolding have a linear dependence on the molar concentration of the denaturant, i.e.:

$$\Delta G_u = \Delta G_{H_2O} + m[\text{GdnCl}] \quad (5)$$

$$\Delta S_u = \Delta S_{H_2O} + s[\text{GdnCl}] \quad (6)$$

$$\Delta H_u = \Delta H_{H_2O} + h[\text{GdnCl}] \quad (7)$$

$$\Delta C_{up} = \Delta C_{p,H_2O} + c[\text{GdnCl}] \quad (8)$$

ΔG_u, ΔS_u, ΔH_u, and ΔC_{up} represent the respective parameters obtained in the presence of a known GdnCl concentration. The denaturant concentration at which $\Delta G_u = 0$ at any temperature is given by C_m, so that $\Delta G_{H_2O} = -C_m m$.

The thermal unfolding curves obtained, using far-UV CD, in the absence and presence of varying concentrations of GdnCl (0.5−5.0 M), were normalized to the fraction folded, f_N (=1 − f_U), using the equation:

$$f_U = Y_o - (Y_f + m_f[D])/\{(Y_u + m_u[D]) - (Y_f + m_f[D])\} \quad (9)$$

where f_U is the fraction unfolded, Y_o is the observed spectroscopic property, and m_f and Y_f are the slope and intercept of the folded state baseline, respectively, while m_u and Y_u are those for the unfolded baseline at denaturant concentration [D]. These unfolding profiles when fitted to eq 4 provide an estimate of ΔH_g, ΔS_g, and ΔC_p at each GdnCl concentration, the temperature of maximum stability (T_s), and the temperature at which the enthalpy is zero (T_h). Additionally, the conformational stability at T_s (ΔG_s) can be obtained for each curve by the equations:

$$\ln(T_g/T_s) = \Delta H_g/T_g\Delta C_p \quad (10)$$

$$T_h = T_g - \Delta H_g/\Delta C_p \quad (11)$$

$$\Delta G_s = \Delta C_p(T_s - T_h) \quad (12)$$

RESULTS

Differential Scanning Calorimetry. A typical scan of ASAI along with the fit of the single transition peak data to a two-state transition model is shown in Figure 2. The transition peak was also observed upon down-scan of the sample, indicating the transition to be thermally reversible (≥90%). Also, even on thermostating for 1 h at 90 °C, that is, well past its T_m value, the scan reappeared to the extent of 80% or more. Also seen in Figure 2 (insets A and B) is the reversibility of ASAI as monitored by CD and fluorescence, respectively. Shown in Table 1 and consistent with the reversibility of the transition, data at higher scan rates exhibit very small increase in T_m and T_p, while ΔH_v remains the same. The protein concentration dependence of T_p for an oligomeric protein undergoing dissociation is related by the equation (*28*):

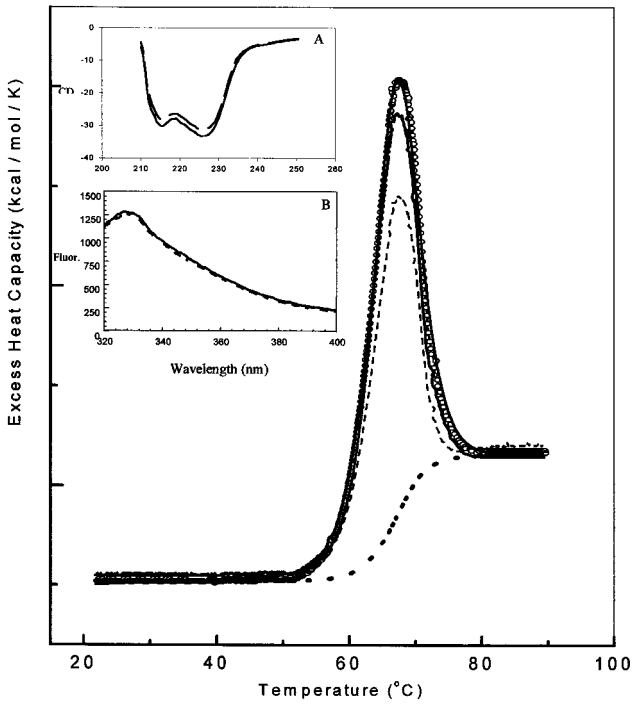

FIGURE 2: Representative DSC scan of 32 μM ASAI at pH 7.5 at a scan rate of 20 °C/h. The data points are shown as open circles (○). The two-state fit is shown as a solid line, while the baseline is shown as a dotted line. The rescan after thermal equilibration of the sample at 90 °C for 1 h is shown as a dashed line. Down-scan of the sample is shown as a thick line. (Inset) Reversibility of ASAI as observed after unfolding in the presence of 6 M GdnCl followed by refolding as monitored by (A) CD and (B) fluorescence. The solid line represents the spectra of the native protein whereas the dashed line represents the refolded protein.

$$\ln[\text{ASAI}] = -\Delta H_v(S)/[RT_p(n - 1)] + \text{constant} \quad (13)$$

where *n* is the number of subunits in the oligomer, [ASAI] is the concentration of the protein oligomer in the native state, and $\Delta H_v(S)$ is the van't Hoff enthalpy obtained from the slope of ln [ASAI] versus $1/T_p$. A plot of ln [ASAI] versus $1/T_p$ is shown in Figure 3 , and the van't Hoff enthalpies calculated from the slope [$\Delta H_v(S)$] are listed in Table 1. The observed increase in the transition temperature with protein concentration highlights the concerted dissociation and unfolding of ASAI. Reasonable agreement between the values of ΔH_v obtained by the two-state fits of the transition data with those determined by a plot of ln [ASAI] versus $1/T_p$ [i.e., $\Delta H_v(S)$ with $n = 2$] validates treatment of the transition as a $A_2 \leftrightarrow 2U$ type transition.[2]

We also recorded DSC thermograms as a function of pH, ranging from 5.0 to 8.0, i.e., under the conditions the protein

[2] The coupled dissociation and unfolding of the ASAI heterodimer can also be represented by the general scheme $AB \leftrightarrow 2U$. As both monomers of the ASAI heterodimer are structurally and functionally equivalent (A = B), the unfolding process is described appropriately by $A_2 \leftrightarrow 2U$.

Table 1: Dependence of DSC Transition Quantities on Concentration of ASAI at pH 7.5[a]

concn (μM)	scan rate (°C h^{-1})	T_m (°C)	ΔH_v (kcal mol^{-1})	ΔH_c (kcal mol^{-1})	$\Delta H_c/\Delta H_v$ ratio	T_p (°C)	$\Delta H_v(S)$ (kcal mol^{-1})
32.0	20.0−90.0	69.8−71.1	112.0−119.0	108.0−136.0	1.08−1.23	68.8−70.9	
4.0	20.0	66.6	112.0	96.4	0.86	66.7	135.0
8.0		67.5	113.0	116.0	1.03	68.5	
16.0		68.9	115.0	118.0	1.03	69.7	
32.0		69.8	117.0	118.0	1.01	69.9	
64.0		69.9	119.0	116.0	0.97	71.7	

[a] Uncertainties in the various parameters listed above are as follows: ±0.1 K for T_m; ±5.6 kcal mol^{-1} for ΔH_v, ΔH_c, and $\Delta H_v(S)$; ±0.9 for $\Delta H_c/\Delta H_v$.

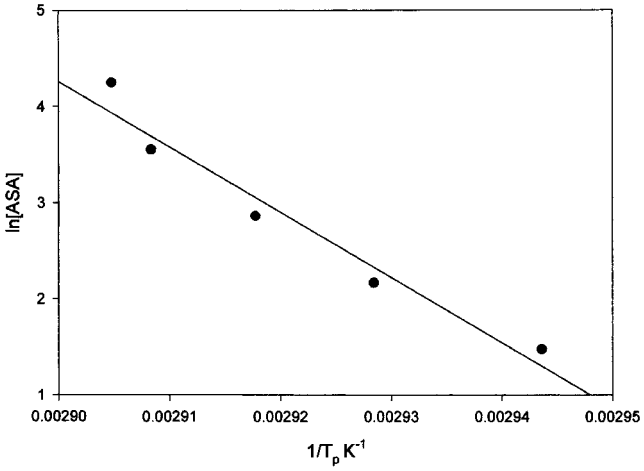

FIGURE 3: Plot of ln [ASA] vs $1/T_p$. The line is the linear least-squares fit of ln [ASAI] to $1/T_p$ with correlation coefficient = 0.96.

Table 2: Thermodynamic Parameters for the Unfolding of ASAI As Monitored by DSC at a Concentration of 32 μM as a Function of pH at a Fixed Scan Rate of 20 °C h^{-1} [a]

pH	T_m (°C)	ΔH_v (kcal mol^{-1})	T_p (°C)
5.0	75.5	132.0	75.7
5.5	74.6	130.0	74.5
5.8	73.9	128.0	72.5
6.0	73.1	125.0	72.3
6.2	72.5	122.0	72.1
6.5	72.2	120.0	71.9
7.0	70.9	118.0	70.1
7.5	69.8	117.0	69.9
8.0	69.2	112.8	68.4

[a] Uncertainties in T_m and ΔH_v are ±0.1 K and ± 5.4 kcal mol^{-1}, respectively.

does not undergo any major structural change. The enthalpy (ΔH_v) obtained as a 'two-state model' fit of the above scans, when plotted against the respective T_m's yielded a slope (3.03 kcal mol^{-1} K^{-1}) which is an estimate of the heat capacity, ΔC_p (Table 2 and Figure 4). This estimate, which corroborates well with the fit of a single scan (=2.82 ± 0.36 kcal mol^{-1} K^{-1}), is considered more accurate owing to the errors associated with the selection of the unfolded baseline (*27*, *29*). Thus, the thermal unfolding of ASAI monitored by DSC was adequately represented by the two-state dissociation model with only two significantly populated states, the folded dimer and the unfolded monomers.

Two-State Unfolding of ASAI. Preliminary insights provided by the DSC scans were fortified by the use of spectroscopic probes to follow the process of unfolding of ASAI. Fluorescence emission spectra of native and fully denatured ASAI, though substantially red-shifted to 344 nm

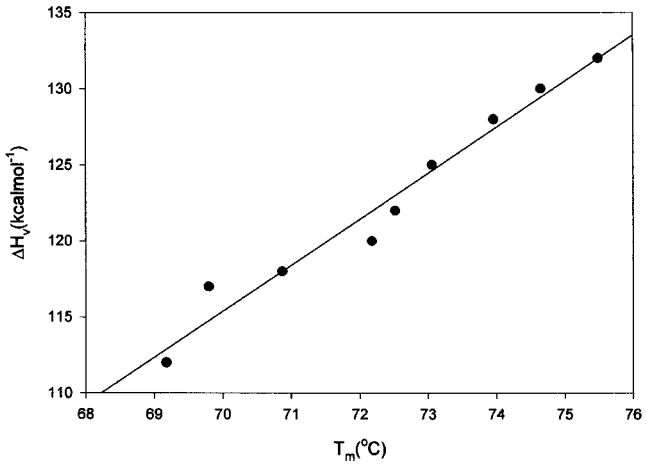

FIGURE 4: Slope of the plot of enthalpy obtained from the individual DSC runs (ΔH_v) vs T_m yields the value of ΔC_p = 3.03 kcal mol^{-1} K^{-1}. The different pH points used for the study were 5.0, 5.5, 5.8, 6.0, 6.2, 6.5, 7.0, 7.5, and 8.0 (correlation coefficient = 0.91).

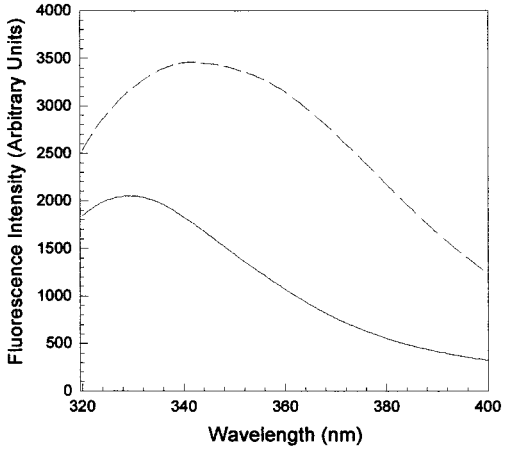

FIGURE 5: Fluorescence emission spectra of native and denatured ASAI (5 μM) at 298 K with (dashed line) and without (solid line) 6 M GdnCl in 20 mM PBS, pH 7.5, show the increase in fluorescence intensity and also the substantial red shift of the λ_{max} from 328 to 344 nm upon unfolding of ASAI. Excitation was at 280 nm. The protein concentration was 3 μM.

from 328 nm, exhibited a marked increase in fluorescence (Figure 5). At pH 4.0, the fluorescence spectra showed a similar increase in fluorescence upon unfolding, but the fluorescence intensity was lower by about 40% (data not shown). Fluorescence in conjunction with CD was employed to monitor the process of unfolding as a function of chemical and thermal denaturation. Analysis of the GdnCl denaturation curves was based on the assumption that only two states, the native and denatured forms, exist at equilibrium; i.e.,

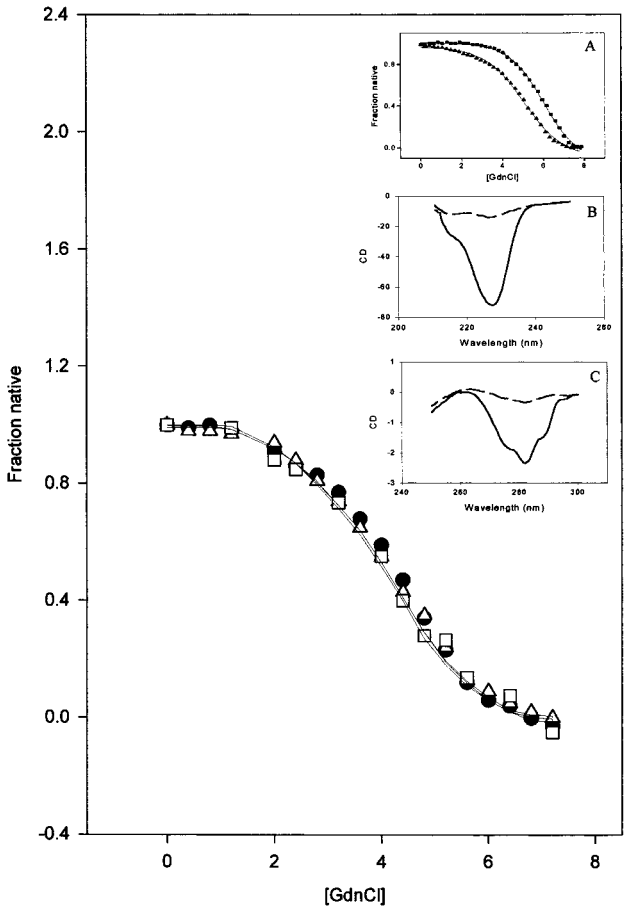

FIGURE 6: (A) GdnCl-induced denaturation curves monitored by fluorescence (●), far-UV CD (△), and near-UV CD (□) at 298 K. The solid line for each profile represents the best fit according to ref *51*. (Inset A) Effect of concentration on the GdnCl-induced denaturation of ASAI as monitored by fluorescence at 298 K. The protein concentrations used were 5 (▲) and 15 μM (■). (Insets B and C) Far- and near-UV CD spectra, respectively, of native ASAI (—) and ASAI denatured with 7.5M GdnCl (– –)

subunit interactions contribute to the overall protein conformational stability. Essentially the unfolding reaction starts with the folded dimer (A_2) and ends with two unfolded monomers. If both folded monomer and folded dimer are significantly populated in the transition region, a three-state model involving equilibrium dissociation of dimer into monomers followed by their melting to random coils may be applied for the unfolding transition of the protein, defined by:

$$A_2 \overset{K_1}{\rightleftharpoons} 2A \overset{K_2}{\rightleftharpoons} 2U \tag{14}$$

where

$$K_1 = [A]^2/[A_2] \text{ and } K_2 = [U]/[A] \tag{15}$$

Transition of this nature may be biphasic or the denaturation curves nonsuperimposable when distinct spectroscopic probes are employed to monitor the unfolding pathway. The GdnCl denaturation profiles obtained by fluorescence and far- and near-UV CD are virtually coincident, supporting the assignment of a simple two-state model involving a single native (A_2) and a single unfolded form (U) for the equilibrium data (Figure 6). This situation simplifies eq 14 to include only folded dimers and unfolded monomers (*8*):

$$A_2 \rightleftharpoons 2U \tag{16}$$

where

$$K_u = [U]^2/[A] \tag{17}$$

Unfolding transitions of this kind would exhibit an increase in protein stability with increase in the protein concentration (Figure 6, inset A). Here, the dimeric state is seen to be significantly populated in the transition zone. From eq 17 and $P_t = [U] + 2[A]$ follows eq 18:

$$K_u = 2P_t \cdot \{f_u^2/(1 - f_u)\} \tag{18}$$

where P_t is the total monomeric protein concentration and f_U the molar fraction of the unfolded protein. Insets B and C of Figure 6 depict the far- and near-UV CD spectra of the native (—) and denatured (– –) protein, respectively, attesting to the absence of any residual structure in the fully denatured protein.

Thermal Unfolding followed by Circular Dichroism. DSC data were complemented with the analyses of thermal denaturation profiles studied by CD. Figure 7A shows the shift in heat denaturation to lower temperatures with increasing GdnCl concentration. At concentrations higher than 5.0 M GdnCl, the protein was fully unfolded, and no transitions were seen. For thermal transitions, the apparent free energy change at any temperature (in the absence and presence of GdnCl) is obtained from eqs 17 and 19:

$$\Delta G = -RT \ln K_{eq} \tag{19}$$

The transitions, characterized by a single sharp change in ellipticity, are typical of a two-state model. Thermodynamic parameters derived from fitting these curves to the van't Hoff analyses show that an increase of GdnCl concentration reduces the thermal stability of the protein (i.e., T_m values) and also the enthalpy change upon unfolding. Analyses of these profiles using eqs 9−11 provide an estimate of ΔH_g, ΔS_g, ΔC_p, ΔG_s, and T_s at each GdnCl concentration (Table 3). Plot of ΔH_g and T_g, obtained above, yields a measure of the apparent $\Delta C_p = 3.01$ kcal mol^{-1} K^{-1} (Figure 7B). The ΔC_p from the least-squares fits of the individual curves using eq 4 increases with increasing GdnCl concentration as plotted in Figure 7C. Moreover, the free energy values obtained from the thermal unfolding profiles of ASAI were used to evaluate the [GdnCl] dependence of the thermodynamic parameters, namely, ΔH_T, ΔS_T, and ΔG_T, as a test of the LEM. These values were calculated for several temperatures between 260 and 350 K using eqs 1−4 to establish their linear relationship with molar concentrations of GdnCl. ΔH_T, ΔS_T, and ΔG_T thus obtained at different temperatures [265 (●), 280 (○), and 295 K (▲)] were plotted with respect to the corresponding GdnCl concentration (Figure 7D−F). ΔH_T and ΔS_T change linearly with GdnCl concentration in a manner that the ΔG_T decreases linearly with respect to GdnCl concentration, conforming to the LEM. The slopes for the plots of ΔH_T and ΔS_T are different at different temperatures. The slopes are −4.83 and −0.023 for ΔH_T and ΔS_T, at 265 K, respectively, while at 295 K they are −2.13 and −0.0134. Increase in the slope with increase in temperature suggests the protein−denaturant interaction to be affected by temperature (*4, 30*). Extrapolation of the linear plots of Figure

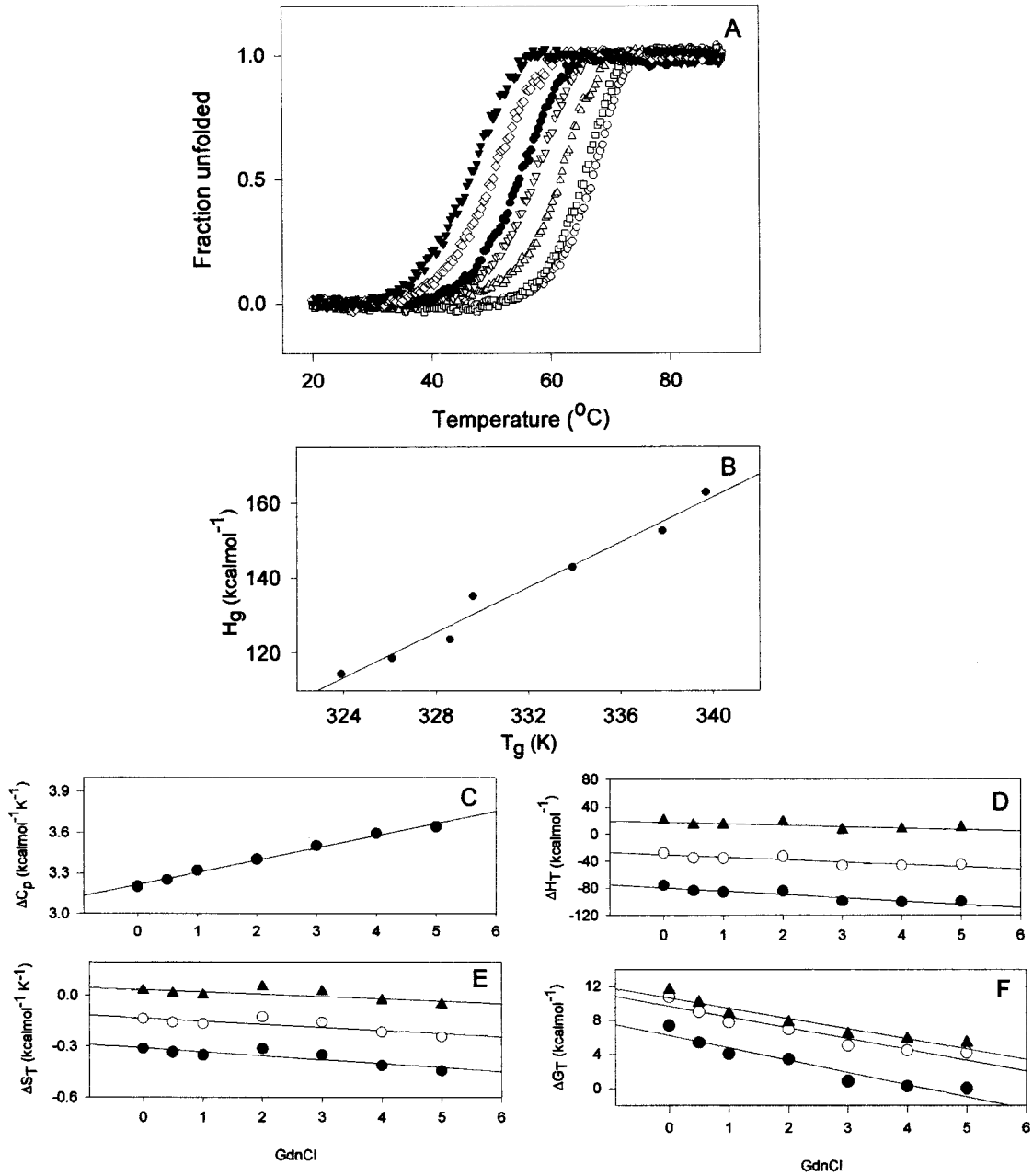

FIGURE 7: (A) Thermal denaturation of ASAI, monitored by far-UV CD at 216 nm. The scans are in the absence (○) and presence of 0.5 (□), 1.0 (△), 2.0 (▽), 3.0 (●), 4.0 (◇), and 5.0 M (▼) GdnCl. A linear extrapolation of the baselines in the pre- and post-transitional regions was used to determine the native fraction of the protein within the transition region by assuming a two-state mechanism for unfolding. (B) The linear relationship, with a slope = 3.01 kcal mol^{-1} K^{-1}, between H_g and T_g is a measure of the apparent heat capacity and has a correlation coefficient = 0.94. (C) [GdnCl] dependence of ΔC_p. (D−F) [GdnCl] dependence of various thermodynamic factors, namely, ΔH_T (D), ΔS_T (E), and ΔG_T (F) at 265 (●), 280 (○), and 295 K (▲). The values plotted were calculated using eqs 1−4.

7D gives the value of ΔH_T at 0 M GdnCl at different temperatures. The values of ΔH_T thus obtained when plotted against the respective temperatures have a slope which is an estimate of $\Delta C_p = 3.32$ kcal mol^{-1} K^{-1} (data not shown).

Equilibrium Unfolding. ΔC_p was also obtained from the unfolding free energies evaluated from the GdnCl denaturation curves recorded at nine temperatures below the thermal transition zone ranging from 283 to 323 K (Figure 8; *4*, *22*). These curves when analyzed using eqs 5, 18, and 19 gave the free energy of unfolding in water [$\Delta G_{(H_2O)}$], as shown in Table 4 and plotted in Figure 9A [open circles (○)], with the assumption that ΔC_p is constant over the temperature range studied. The unfolding free energy ΔG_T at temperature T is given by eq 4. The data shown in Figure 9A were least-squares-fit to eq 4. It provides an estimate of T_g ΔH_g and ΔC_p as 339.4 K, 174.1 kcal mol^{-1} and 3.41 ± 0.32 kcal mol^{-1} K^{-1}, respectively, which is in good agreement with the value obtained from the thermal transitions monitored by CD. The closed circles (●) in Figure 9A represent the ΔG_u values calculated from the thermal denaturation experiments shown in Figure 7A, assuming the two-state model. Coincidence of the two data set points, namely, thermal and isothermal melts, reiterates the LEM to appropriately define the protein−denaturant interaction. C_m, defined by the equation $-\{RT \ln [\text{protein}] + \Delta G_{(H_2O)}\}/m$, plotted as a function of temperature shows the protein to be less stable above and below 293 K (Figure 9B). This variation in the value of C_m can be accounted for by shorter protein baselines at

Table 3: Thermodynamic Parameters for the Thermal Unfolding of ASAI at pH 7.5 Monitored by Far-UV CD at 216 nm[a]

[GdnCl] (M)	T_g (K)	ΔH_g (kcal mol^{-1})	ΔS_g (kcal mol^{-1} K^{-1})	ΔC_p (kcal mol^{-1} K^{-1})	T_s (K)	ΔG_s (kcal mol^{-1})
0.0	339.4	173.2	0.51	3.20	289.37	13.10
0.5	337.2	152.8	0.45	3.25	293.32	10.17
1.0	333.8	142.5	0.43	3.32	293.52	8.78
2.0	329.3	136.2	0.41	3.40	291.58	7.96
3.0	328.7	123.9	0.38	3.50	295.14	6.44
4.0	326.3	117.9	0.36	3.59	295.06	5.74
5.0	323.7	114.8	0.35	3.64	293.65	5.42

[a] The values of T_g, ΔH_g, and ΔC_p were derived from the stability curves using eq 4. ΔS_g was determined using $\Delta S_g = \Delta H_g/T_g$. T_s is the temperature of maximum free energy conformational stability, obtained from $T_s = T_g/\{\exp(\Delta H_g/\Delta C_p T_g)\}$. ΔG_s was calculated by the substitution of T with T_s in eq 4. Experimental errors from the least-squares fit are as follows: ±0.42 kcal mol^{-1} K^{-1} for ΔC_p, ±8.9 kcal mol^{-1} for ΔH_g, ±0.49 kcal mol^{-1} K^{-1} for ΔS_g, ±0.5 K and ±2 K for T_g and T_s, respectively, and ±0.62 kcal mol^{-1} for ΔG_s.

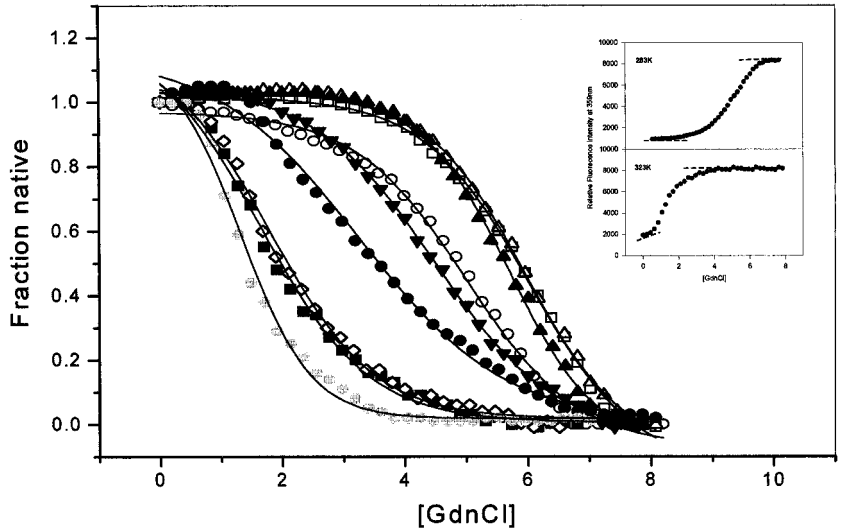

FIGURE 8: GdnCl-induced denaturation curves at nine different tempetatures ranging from 283 to 323 K {283 (○), 288 (□), 293 (△), 298 (▲), 303 (▼), 308 (●), 313 (■), 318 (◆), and 323 (gray circles)} monitored by fluorescence at 359 nm. The solid line for each profile is the best fit according to eq 4. (Inset) Representative isothermal melts at (A) 283 and (B) 323 K, with the dashed line highlighting the baseline selected for the fits.

Table 4: Analysis of the Isothermal GdnCl Denaturation Curves at Different Temperatures[a]

temp (K)	C_m (M GdnCl)	$\Delta G_{(H_2O)}$ (kcal mol^{-1})	m (kcal mol^{-1} M^{-1})
283	4.90	12.78	−2.61
288	5.84	13.03	−2.23
293	5.84	13.13	−2.25
298	5.60	12.90	−2.30
303	4.62	12.21	−2.64
308	3.40	10.90	−3.21
313	2.41	9.65	−4.00
318	1.99	7.74	−3.89
323	1.50	5.75	−3.83

[a] Experimental errors are ±0.1 M for C_m, ±1.3 kcal mol^{-1} for $\Delta G_{(H_2O)}$, and ±0.41 kcal mol^{-1} M^{-1} for m.

extremes of temperature, especially at higher temperatures. The value of m, though marginally lower than that for a protein of this size, appears to be independent of temperature over the range studied (Figure 9C).

DISCUSSION

Structural Characteristics of ASAI. The Amaryllidaceae and Alliaceae families of lectins including ASAI exhibit similar tertiary structural fold and exist as oligomeric proteins (mostly dimers or tetramers). The structural basis of the differences in their states of oligomerization is at present incompletely understood. One of the ways to understand differential oligomeric levels for these proteins is to characterize their folding behavior and conformational stabilities. The three-dimensional structure reveals that dimerization in ASAI occurs by a strand exchange process wherein three strands of the first sheet of one subunit interact with a strand that crosses over from the adjacent subunit. Such a crossover, observed in only a few proteins so far, has a major consequence for stabilizing the dimer, as it enables extensive interactions between the two subunits (Figure 1). The central region of the β-prism II fold of ASAI constitutes the hydrophobic core stacked with conserved nonpolar residues, viz., seven leucines, three tryptophans, two phenylalanines, two valines, and one methionine. The three tryptophans, Trp41, Trp74, and a Trp103 from the dimer-related subunit, a consequence of strand exchange, are unique as they do not stack but are arranged at an angle of 120° to each other with their side chains oriented into the β-barrel core (*13*).

Principle Observations from This Study. Denaturation profiles of ASAI recorded at several temperatures with and without GdnCl unravel its unfolding in terms of the dissociation of the dimer into its constituent monomeric subunits. The principle observations from these studies are the following: (1) The unfolding of ASAI is a simple two-state process, namely, $A_2 \leftrightarrow 2U$. (2) No hysteresis for the unfolding/refolding reaction is observed. (3) The ΔC_p of its

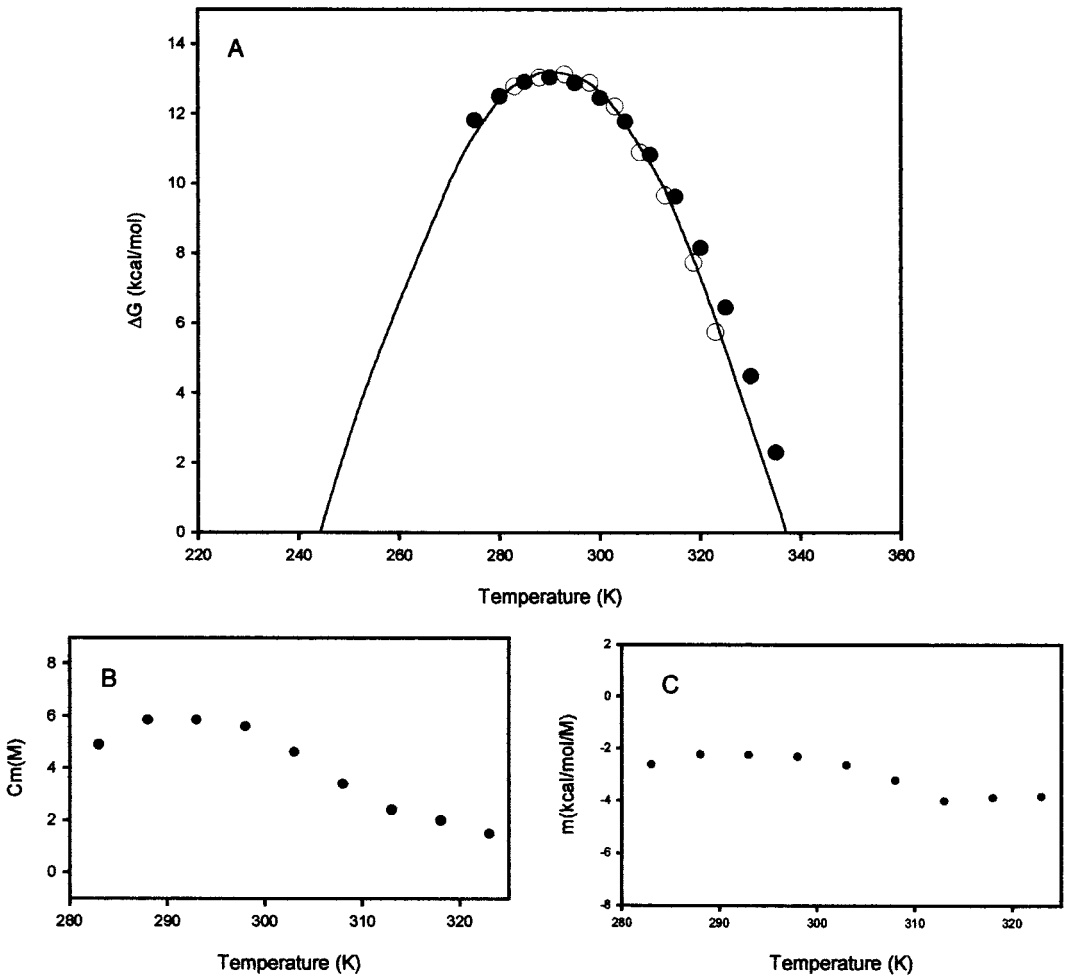

FIGURE 9: (A) Unfolding free energy as a function of temperature. The open circles (○) are $\Delta G_{(H_2O)}$ values deduced from the isothermal GdnCl melts at various temperatures ranging from 283 to 323 K. ΔG values of ASAI as a function of temperature at pH 7.5 were estimated from eq 4 using a value of $T_g = 339.4$ K. ΔG for the curve indicated by the solid line is the best fit obtained according to eq 4 using a value of 3.41 kcal mol^{-1} K^{-1} for ΔC_p and 174.1 kcal mol^{-1} for ΔH_g. The closed circles (●) depict the ΔG values obtained from the thermal unfolding in the absence of GdnCl monitored by far-UV CD. (B) C_m and (C) m as a function of temperature in the range 283−323 K.

unfolding is mostly independent over a wide range of temperature. (4) Detailed analyses of the stability curves is consistent with the LEM for the thermodynamic stability of ASAI. (5) Importantly, the unfolded monomers induced by either heat or chemical denaturation are effectively equivalent, indicating that the unfolded states generated by them are devoid of appreciable residual structure. (6) It provides insight into the hydrophobic core of the native protein. Complete reversibility of the unfolding process of ASAI and observation of good correlation between the thermodynamic parameters obtained independently from calorimetric, spectroscopic, and isothermal melts substantiate the assumption of the two-state unfolding model. Moreover, the availability of its three-dimensional structure fulfills all criteria for ASAI to serve as an excellent model to investigate the thermodynamics and mechanism of protein folding in multimeric proteins. This merits even more attention as the oligomeric proteins often do not exhibit reversible denaturation. Additionally, to our knowledge, this is the first report of such studies on a strand-exchange-stabilized all-β-sheet protein.

Quenching of the Three Trp's in the β-Barrel Core. The λ_{max} of the unfolded protein is significantly red-shifted at 344 nm with respect to that of the folded protein at 328 nm (Figure 5). Moreover, the λ_{max} of the unfolded protein, besides being close to the λ_{max} of tryptophan as a free amino acid, shows a substantial 70% increase in fluorescence intensity. This quenching effect, among the tryptophans, is removed upon complete unfolding of ASAI, leading to the dramatic increase in fluorescence. The quenched tryptophan fluorescence in the native protein can be accounted for by the presence either of a (i) water molecule in the hydrophobic core of the β-barrel or of a (ii) charged amino acid side chain within striking distance or by (iii) self-quenching among the tryptophans. Examination of the three-dimensional structure failed to reveal any trapped water molecule(s) in the hydrophobic core. The atomic coordinates of the ASAI structure revealed the presence of a histidine at distances of 8.5 and 7.1 Å (between NE1 of Trp and ND1 of His) from Trp74 and Trp103, respectively. These two observations from the crystal structure thus leave us to suggest that quenching of the intrinsic tryptophan fluorescence is caused partly, about 40%, by the charged His77. In addition, self-quenching, due to the geometry of the tryptophans, within van der Waals distance in the center of the barrel, appears to account significantly (60%) for the increased fluorescence upon unfolding.

ASAI Unfolding Conforms to the Norms of LEM. The chaotrope-induced equilibrium unfolding of ASAI, followed

by fluorescence far- and near-UV CD, shows no evidence for the existence of stable intermediates, substantiating the assumption of a two-state transition (Figure 6A,B). A combination of GdnCl and thermal denaturation experiments on ASAI was carried out to test whether the LEM or the denaturant binding model of protein unfolding is applicable for this all-β-sheet protein (*31*−*33*). While the LEM predicts a linear decline in the conformational stability of the protein with increasing denaturant concentration, the binding model assumes a logarithmic dependence. The values documented in Table 3 were used to estimate the dependence of the thermodynamic parameters on GdnCl concentration using eqs 1−4. Their linearity as a function of increasing GdnCl concentration conform to the norms of LEM (Figure 7D−F). The change in the value of ΔC_p with increasing concentration of GdnCl (Figure 7C) is similar to the trend seen for barstar (*1*), pea lectin (*8*), and uracil−DNA glycosylase inhibitor (*30*) and unlike the Hpr (*2*), which shows a linear decrease in ΔC_p, while β-lactoglobulin shows no regular trend with increasing concentration of the denaturant (*34*). The coincidence of the two data sets from thermal and isothermal GdnCl melts validates the baseline selected to fit the denaturation profiles (Figures 7A, 8, and 9A; Tables 3 and 4). The parameters obtained from the stability curve provide a means to analyze the effect of [GdnCl] on ΔH, ΔG, and ΔS at any given temperature as detailed under Results.

Another parameter obtained from the CD melts, the '*m*' value, reveals a value slightly lower than expected for a protein of similar size at room temperature (*35*). This can be due to formation of a compact denatured state or change in the population of equilibrium folding intermediate (*36*), both of which are incidentally ruled out by the consistency between the ΔC_p values derived from the structural data and the denaturation experiments (discussed below) and by the perfect superimposition of the melts using distinct spectroscopic probes, respectively.[3]

Absence of Cold Denaturation. These parameters also reveal the absence of cold denaturation for ASAI in the accessible temperature range. Though ASAI satisfies one of the criteria for cold denaturation, as the temperature of its maximum stability is well above 273 K, its ΔG_s, at 13.13 kcal mol^{-1}, is moderate for a protein of 25 kDa. It fails to conform to the important criterion of a low value for the ratio of $\Delta H/\Delta C_p$. For ASAI, ΔH at 293 K (temperature of its maximum stability) is 13.36 kcal mol^{-1}, which is quite high, while the ΔC_p, obtained by a variety of methods, is ~3.0 kcal mol^{-1} K^{-1} (*5*, *37*, *38*). Consequently, $\Delta H/\Delta C_p$ is very high, explaining the absence of cold denaturation in ASAI in the observable temperature range. These studies allow us to validate further the correlation between the occurrence of cold denaturation in the accessible temperature range and the low values of the ratio of the measurable thermodynamic parameters, i.e., $\Delta H/\Delta C_p$.

Calculation of ΔC_p from the Accessible Surface Area. Analysis of thermodynamic data for a large repertoire of monomeric proteins shows correlation among their ΔC_p, ΔH, ΔS, protein size, and accessible surface area buried upon folding (ΔASA) (*35*, *37*−*42*). The total ASA in the crystal structure of garlic lectin determined using the program NACCESS was 10 117.1 Å^2, wherein the polar and nonpolar contributions are respectively 4898.2 and 5218.9 Å^2 (*43*). Upon dimerization, the loss of apolar ASA (the difference between the apolar ASA in the unfolded and folded state) is 16 205.8 Å^2 and polar ASA is 9317.8 Å^2. The ASA in the folded state was calculated using a probe radius of 1.4 Å^2 and a slice width of 0.25 Å^2, while the unfolded state was modeled as the sum of extended Ala-X-Ala tripeptides, where X is any amino acid (*44*, *45*). Burial of almost 77% of the apolar ASA suggests that the hydrophobic interactions drive the dimerization of the protein. ΔC_p can be parametrized as a function of changes in the polar and nonpolar solvent-accessible area:

$$\Delta C_p = \Delta C_{p,\mathrm{ap}} \Delta \mathrm{ASA}_{\mathrm{ap}} + \Delta C_{p,\mathrm{pol}} \Delta \mathrm{ASA}_{\mathrm{pol}} \qquad (20)$$

Using eq 20, the ΔC_p of unfolding for garlic lectin is calculated to be 3.51 kcal mol^{-1} K^{-1}, which is in excellent agreement with the experimentally determined values (3.2 ± 0.28 kcal mol^{-1} K^{-1}).[4] Analysis of unfolding curves, obtained by physical means, using eq 4, assumes ΔC_p to be independent of temperature, thus underestimating ΔC_p, accounted for by the negative enthalpy of interaction between GdnCl and the protein surface area exposed to solvent upon unfolding. These data thus suggest attainment of a completely unfolded state for ASAI, in contrast to majority of proteins where some residual structure still persists in the denatured state (*46*−*48*).

Remarkably, the dimerization in ASAI occurs by a strand exchange process also referred to as domain swapping, which appears to be a mode of oligomerization in proteins such as diphtheria toxin, RNase A, BS Rnase, βB2-crystallin, IFN-γ, IL-5, and p13suc1, to name a few (*49*). Such "entangling alliances", observed in a few proteins so far, is implicated in stabilizing the dimer by primary as well as secondary interdomain interfacial contacts between the two subunits (*49*). Disruption of such an interaction between subunits may be sufficient to destabilize the folded dimeric structure yielding the unfolded monomers as observed experimentally in these studies.

CONCLUSIONS

In this paper, the folding and stability of ASAI when investigated as a function of pH, temperature, and GdnCl by intrinsic fluorescence, far-UV CD, and DSC provide an estimate of the heat capacity (3.2 kcal mol^{-1} K^{-1}). This ΔC_p of ASAI is consistent with those determined from a calculation of the surface area buried upon dimerization employing the parameters derived from the crystal structure and compares well with that of the Arc repressor dimer (1.6 kcal mol^{-1} K^{-1}), composed of two 53 residue polypeptide chains, exactly half the size of ASAI (*4*). In addition, we show the thermal unfolding of ASAI to be a two-state process in which the folded dimer unfolds cooperatively by a concerted mechanism into unfolded monomers. Under all conditions studied, neither the partially folded dimers nor the folded monomers/partially folded species thereof could be detected.

[3] Factors other than the accessible surface area might contribute to the '*m*' value, thus making it difficult to correlate the '*m*' value with the molecular size (*50*).

[4] For averaging, the ΔC_p obtained from the single DSC scan was not considered as it is prone to large errors.

In addition, the fluorescence and CD data, too, revealed the presence of only two significantly populated states. Since states other than the folded dimers or the unfolded monomers cannot be detected, one is led to conclude that the energy of stabilization of the dimer derives primarily from the cooperative interactions along the monomer−monomer contact interface of the ASAI dimer. Once these interactions are eliminated, the individual chains do not retain any appreciable secondary or tertiary structure. The hydrophobic effect appears to be the major force for the stability of the ASAI dimer. Furthermore, the unfolded monomers of ASAI are devoid of any residual structure, explaining an excellent correlation between the theoretically calculated accessibility surface area buried upon dimerization and ΔC_p values. Moreover, these data also shed light on the fluorescence of its tryptophans both in the folded and in the unfolded states.

ACKNOWLEDGMENT

We thank Drs. Raghavan Varadarajan and D. Chatterji for critical reading of the manuscript. We also thank S. Sri Krishna, Suvobrata Chakravarty, and S. Balaji for helpful discussions.

REFERENCES

1. Agashe, V. R., and Udgaonkar, J. B. (1995) *Biochemistry 34*, 3286−3299.
2. Nicholson, E. M., and Scholtz, J. M. (1996) *Biochemistry 35*, 11369−11378.
3. Neet, K. E., and Timm, D. E. (1994) *Protein Sci. 3*, 2167−2174.
4. Johnson, C. R., Morin, P. E., Arrowsmith, C. H., and Freire, E. (1995) *Biochemistry 34*, 5309−5316.
5. Bowie, J. U., and Sauer, R. T. (1989) *Biochemistry 28*, 7139−7143.
6. Dill, K. A., Bromberg, S., Yue, K., Fiebig, K. M., Yee, D. P., Thomas, P. D., and Chan, H. S. (1995) *Protein Sci. 4*, 561−602.
7. Matthews, R. R. (1993) *Annu. Rev. Biochem. 62*, 653−683.
8. Ahmad, N., Srinivas, V. R., Reddy, G. B., and Surolia, A. (1998) *Biochemistry 37*, 16765−16772.
9. Hester, G., Kaku, H., Goldstein, I. J., and Wright, C. S. (1995) *Nat. Struct. Biol. 2*, 472−479.
10. Sauerborn, M. K., Wright, L. M., Reynolds, C. D., Grossman, J. G., and Rizkallah, P. J. (1999) *J. Mol. Biol. 290*, 185−199.
11. Wood, S. D., Wright, L. M., Reynolds, C. D., Rizkallah, P. J., Allen, A. K., Peumans, W. J., and Van Damme, E. J. M. (1999) *Acta Crystallogr. D55*, 1264−1272.
12. Chantalat, L., Wood, S. D., Rizkallah, P. J., and Reynolds, C. D. (1996) *Acta Crystallogr. D52*, 1146−1152.
13. Chandra, N. R., Ramachandraiah, G., Bachhawat, K., Dam, T. K., Surolia, A., and Vijayan, M. (1999) *J. Mol. Biol. 285*, 1157−1168.
14. Barre, A., Van Damme, E. J. M., Peumans, W. J., and Rouge, P. (1996) *Plant Physiol. 112*, 1531−1540.
15. Van Damme, E. J. M., Astoul, C. H., Barre, A., Rouge, P., and Peumans, W. J. (2000) *Eur. J. Biochem. 267*, 5067−5077.
16. Shankarnarayanan, R., Sekar, K., Banerjee, R., Sharma, V., Surolia, A., and Vijayan, M. (1996) *Nat. Struct. Biol. 3*, 596−602.
17. Murzin, A. G., Lesk, A. M., and Chothia, C. (1992) *J. Mol. Biol. 223*, 531−543.
18. Van Damme, E. J. M., Smeets, K., Torrekens, S., Van Leuven, F., Goldstein, I. J., and Peumans, W. J. (1992) *Eur. J. Biochem. 206*, 413−420.
19. Goldstein, I. J., and Hayes, C. E. (1978) *Adv. Carbohydr. Chem. Biochem. 35*, 127−340.
20. Pace, C. N., and Laurents, D. V. (1989) *Biochemistry 28*, 2520−2525.
21. Dam, T. K., Bachhawat, K., Rani, P. G., and Surolia, A. (1998) *J. Biol. Chem. 273*, 5528−5535.
22. Schwarz, F. P. (1988) *Biochemistry 27*, 8429−8436.
23. Schwarz, F. P., Puri, K. D., Bhatt, R. G., and Surolia, A. (1993) *J. Biol. Chem. 268*, 7668−7677.
24. Becktel, W. J., and Schellman, J. A. (1987) *Biopolymers 26*, 1859−1877.
25. Schellman, J. A. (1978) *Biopolymers 17*, 1305−1322.
26. Schellman, J. A. (1987) *Biopolymers 26*, 549−559.
27. Privalov, P. L., and Khechinashvili, N. N. (1974) *J. Mol. Biol. 86*, 665−684.
28. Fukuda, H., Sturtevant, J. M., and Quiocho, F. A. (1983) *J. Biol. Chem. 258*, 13193−13198.
29. Ladbury, J. E., Kishore, N., Hellinga, H. W., Wynn, R., and Sturtevant, J. (1994) *Biochemistry 33*, 3688−3692.
30. Reddy, G. B., Purnapatre, K., Lawrence, R., Roy, S., Varshney, U., and Surolia, A. (1999) *Eur. J. Biochem. 261*, 610−617.
31. Schellman, J. A. (1990) *Biophys. Chem. 37*, 121−140.
32. Schellman, J. A., and Grassner, N. C. (1996) *Biophys. Chem. 59*, 259−275.
33. Tanford, C. (1970) *Adv. Protein Chem. 21*, 1−95.
34. Girko, Y. V., and Privalov, P. L. (1992) *Biochemistry 31*, 8810−8815.
35. Myers, J. K., Pace, C. N., and Scholtz, J. M. (1995) *Protein Sci. 4*, 2138−2148.
36. Hammack, B., Attfield, K., Clayton, D., Dec, E., Dong, A., Sarisky, C., and Bowler, B. E. (1998) *Protein Sci. 7*, 1789−1795.
37. Ganesh, C., Shah, A., Swaminathan, C. P., Surolia, A., and Varadarajan, R. (1997) *Biochemistry 36*, 5020−5028.
38. Paanse, V. G., Swaminathan, C. P., Aloor, J. J., Surolia, A., and Varadarajan, R. (2000) *Biochemistry 39*, 2362−2369.
39. Janin, J. (1976) *J. Mol. Biol. 105*, 13−14.
40. Livingstone, J. R., Spolar, R. S., and Record, M. T., Jr. (1991) *Biochemistry 30*, 4237−4244.
41. Spolar, R. S., Ha, J. H., and Record, M. T. (1989) *Proc. Natl. Acad. Sci. U.S.A. 86*, 8382−8385.
42. Ooi, T., Oobatake, M., Nemethy, G., and Scheraga, H. A. (1987) *Proc. Natl. Acad. Sci. U.S.A. 84*, 3086−3090.
43. Hubbard, S. J., and Thornton, J. M. (1993) 'NACCESS' Computer Program, Department of Biochemistry and Molecular Biology, University College London.
44. Luque, I., and Freire, E. (1998) *Methods Enzymol. 295*, 100−127.
45. Baker, B. M., and Murphy, K. P. (1998) *Methods Enzymol. 295*, 294−315.
46. Makhatadze, G. I., and Privalov, P. L. (1992) *J. Mol. Biol. 226*, 491−505.
47. Robinson, D. R., and Jencks, W. P. (1965) *J. Am. Chem. Soc. 87*, 2462−2470.
48. Schonert, H., and Stroth, L. (1981) *Biopolymers 20*, 817−831.
49. Bennett, M. J., Choe, S., and Eisenberg, D. (1995) *Proc. Natl. Acad. Sci. U.S.A. 91*, 3127−3131.
50. DeKoster, G. T., and Robertson, A. D. (1997) *Biophys. Chem. 64*, 59−68.
51. Santoro, M. M., and Bolen, D. W. (1988) *Biochemistry 27*, 8063−8068.

BI0027783